Hyperfine interactions and magnetic properties of amorphous Fe-Sb alloys

C. L. Chien, Gang Xiao, and K. M. Unruh*
Department of Physics and Astronomy, The Johns Hopkins University, Baltimore, Maryland 21218
(Received 2 May 1985)

We present a systematic investigation of amorphous Fe_xSb_{100-x} alloys fabricated over a wide composition range ($3 \leq x \leq 80$). For the Fe-rich samples, the concentration dependence of the isomer shift is compatible with the Miedeme—van der Woude model, while a large discrepancy is found in samples with Fe concentrations less than 50 at. %. This suggests that a new term characteristic of *sp* elements is necessary in that model. The electric quadrupole splittings have been studied. A particularly striking feature comes from the discovery that the quadrupole splitting of crystalline *x*-$FeSb_2$ is larger than that of its amorphous counterpart *a*-$FeSb_2$ by a factor of 3 at both 4.2 and 300 K. Such a difference in quadrupole splitting is the largest ever found in Fe—*sp*-element and Fe—transition-element amorphous alloys. The magnetic ordering temperatures of the Fe-Sb alloys have been determined. At $x > 60$, samples exhibit mainly ferromagnetic ordering, while below $x = 60$, spin-glass behavior has been observed. The effective magnetic hyperfine field H_{eff}, and hence the effective magnetic moment, of the Fe-Sb alloys increase monotonically with Fe concentration at about $x = 47$. The distributions of magnetic hyperfine field $P(H)$ are also presented and discussed.

I. INTRODUCTION

Metallic amorphous alloys can be fabricated by various ways, of which the vapor-quench and liquid-quench methods are the most commonly used.[1,2] Liquid-quench methods can produce large amounts of material, but suffer from the restriction that the amorphous state can be achieved only for compositions near a deep eutectic in the alloy phase diagram. Vapor-quench techniques, with their inherently higher quenching rates, are capable of making amorphous alloys over a much wider composition range. This is much to be desired in studies of the physical properties of amorphous alloys in relation to composition.

The structural disorder in amorphous alloys introduces a large number of nonequivalent atomic sites which are generally responsible for the distributions of various physical parameters such as hyperfine interaction, magnetic moment, and exchange interaction. By studying these modified physical parameters in amorphous alloys and comparing them with those of the crystalline alloys, one can gain much insight into the structure of amorphous alloys as well as the influence of structural disorder on the physical properties. Mössbauer spectroscopy is a very useful technique for this purpose.[3–5] It has been widely employed in the study of hyperfine interactions, chemical bonding, charge distribution, and magnetic properties in amorphous alloys.

Two classes of amorphous alloys, transition-metal—transition-metal and transition-metal—*sp*-element, have received considerable interest from both practical and fundamental standpoints. In the latter case, amorphous alloys of Fe combined with different *sp* elements of group III*B* and IV*B* such as B, C, Si, Ge, and Sn have been very extensively studied. However, the results of Fe—group-V*B* (e.g., Sb) amorphous alloys remain scarce. Mössbauer data of amorphous Fe_xSb_{100-x} alloys within the range of $10 \leq x \leq 47$ were reported in a brief paper by Shigematsu *et al.*[6] Information, especially that on magnetic properties, is very limited due to the narrow range of the amorphous phase.

In this study, we have taken full advantage of the vapor-quench method in successfully making amorphous Fe-Sb alloys over a wide composition range, and performed a systematic study of the hyperfine interactions and magnetic properties in relation to composition. The very unusual electrical conductivity behavior will be discussed elsewhere.

II. EXPERIMENTAL

The samples in this study were fabricated by a high-rate magnetically assisted sputtering system. The sputtering targets were made from a homogeneous mixture of pure Fe (99.9%) and Sb (99.5%). The vacuum before sputtering was in the (10^{-7}—10^{-8})-Torr range. All the films were deposited onto liquid-nitrogen-cooled substrates of copper or Kapton with Ar as the sputtering gas. The sputtering rate was about 500—1000 Å/min and samples were made with thicknesses of 5—15 μm. The crystalline *x*-FeSb and *x*-$FeSb_2$ samples were obtained commercially.

The structure of the samples was determined by using an energy-dispersive x-ray spectrometer. It was found that samples with $3 \leq x \leq 80$ are amorphous and those beyond $x = 80$ are crystalline. $Fe_{85}Sb_{15}$ was confirmed to have a bcc structure. The substrate temperature played an important role in achieving the amorphous phase over such a wide composition range. It has been reported[6] that the formation of amorphous metallic Fe-Sb alloys is possible within a smaller range of $10 \leq x \leq 47$ when the substrate temperature is maintained at room temperature. In

the present case, by using a liquid-nitrogen-cooled substrate and magnetically confined plasma (minimizing secondary electron bombardment of the substrate), we have expanded the amorphous-phase range dramatically. We also tried to fabricate thick amorphous pure-Sb films, but the amorphous structure could not be maintained at room temperature. This is consistent with the claims that amorphous Sb begins to crystallize at room temperature once its thickness exceeds a critical value of about 250 Å.[7] However, a few percent of Fe is capable of stabilizing the amorphous state.

The hyperfine interactions were studied by a conventional Mössbauer spectrometer with a ^{57}Co-in-Rh source. Most of the data analysis was done on a VAX-11/780 computer. Magnetization measurements were performed using a SHE superconducting quantum-interference device magnetometer. The magnetic ordering temperatures were determined either by the onset of the magnetic hyperfine interaction or by magnetization measurements under a small external magnetic field.

III. RESULTS AND DISCUSSIONS

A. Isomer shift (δ)

Mössbauer spectra of a-Fe_xSb_{100-x} at 300 and 4.2 K are shown in Figs. 1 and 2. The mean isomer shift was determined from the centroid of either the doublet or the sextuplet spectrum. The data of the isomer shifts (relative to α-Fe at 300 K) at 4.2 and 300 K for amorphous Fe-Sb alloys are presented in Fig. 3 as open circles and squares, respectively. Also shown are the results of the crystalline compounds x-FeSb, x-$FeSb_2$, and crystalline alloys

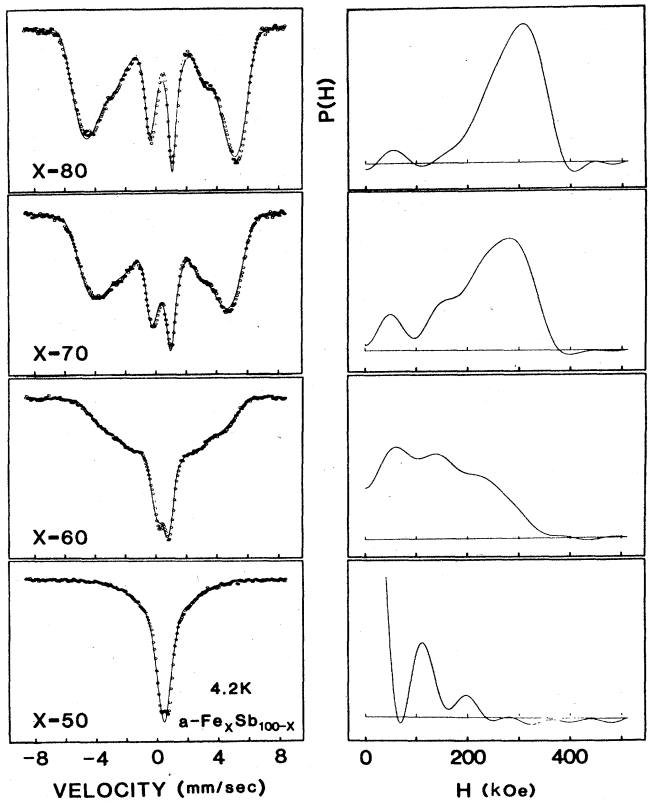

FIG. 2. Mössbauer spectra and deduced magnetic hyperfine field distribution of amorphous Fe-Sb alloys at 4.2 K.

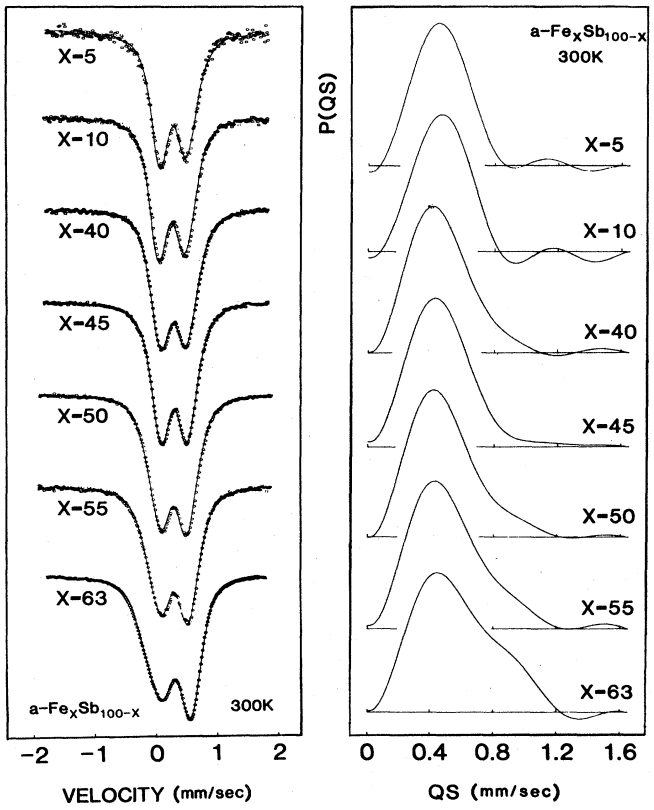

FIG. 1. Mössbauer spectra and deduced quadrupole splitting distribution P(QS) of amorphous Fe-Sb alloys at 300 K.

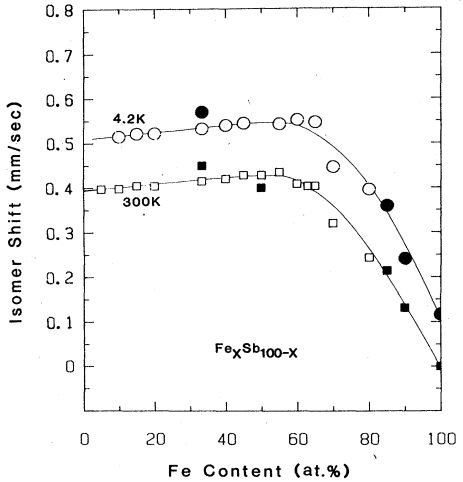

FIG. 3. Isomer shifts (relative to α-Fe) of amorphous Fe_xSb_{100-x} alloys and some crystalline Fe-Sb samples at 4.2 and 300 K. Open squares and circles are data of amorphous samples and solid squares and circles are data of crystalline samples.

($x \geq 85$) as solid circles and squares.

The composition dependences of isomer shifts are very similar at 4.2 and 300 K, except that the curve for 4.2 K is shifted upwards by nearly a constant over the entire composition range due to the second-order Doppler effect. Noticeably, both curves show small composition dependence at $x \leq 60$ and decrease sharply when the composition exceeds 60 at. % of Fe.

In order to interpret the isomer shift of amorphous Fe-Sb alloys, we turn to the Miedema—van der Woude model,[8] which is based on an empirical model of heat of formation of binary alloys and gives satisfactory description of ^{197}Au isomer shift in various alloys containing Au. This model has also been applied to Fe-based amorphous alloys as well.[9–11] According to this model, the extreme isomer shift (relative to α-Fe) for ^{57}Fe nuclei in a binary system Fe-A is given by

$$\delta_{FeA} = P(\phi_A - \phi_{Fe}) + Q(n_A - n_{Fe})/n_{Fe} \ . \quad (1)$$

The value of δ_{FeA} is realized when ^{57}Fe atoms are completely surrounded by dissimilar atoms, i.e., when the concentration of Fe in the binary alloy approaches zero. ϕ is the electronegativity parameter which is related to the value of the macroscopic work function, while n is the electron density at the boundary of the Wigner-Seitz cells of the pure element. Relation (1) tells us that the ^{57}Fe isomer shift is determined by two terms, a charge-transfer term and a cell-electron-density—difference term. Electrons tend to flow from atoms with smaller electronegativity to those with higher ones. On the other hand, the requirement that the electron density at the boundary of dissimilar atomic cells should be continuous forces atoms to redistribute their intra-atomic charges. For transition-metal elements, the latter is accomplished by s-d electron conversion. The competition between charge transfer and intra-atomic charge redistribution is represented by P and Q, which have different signs and are regarded as constants for a given class of Fe alloys.

In the Miedema—van der Woude model it is assumed that the Fe isomer shift of an alloy at a given composition is proportional to the relative contact area of Fe with its neighboring A atoms, i.e.,

$$\delta(x) = C_A(x)\delta_{FeA} \ , \quad (2)$$

where $C_A(x)$, the so-called surface-area concentration of A surrounding Fe, is given by

$$C_A(x) = \frac{(1-x)V_A^{2/3}}{xV_{Fe}^{2/3} + (1-x)V_A^{2/3}} \ . \quad (3)$$

The surface-area concentration for Fe is simply $C_{Fe}(x) = 1 - C_A(x)$, where V_{Fe} and V_A are the molar volumes. As evident from Eq. (2), when the isomer-shift data are plotted as a function of C_{Fe}, one should obtain a *straight line* from δ_{FeA} at $C_{Fe} = 0$ to 0 at $C_{Fe} = 1$. The relevant parameters for Fe and Sb are listed in Table I. From these parameters, together with $P = 0.75$ and $Q = -1.65$ obtained from Fe—transition-metal amorphous alloys,[10] Eq. (1) gives $\delta_{FeSb} = 0.66$ mm/sec.

Figure 4 shows the isomer shift of Fe-Sb alloys as a function of the surface-area concentration of Fe. On the Fe-rich side [$C_{Fe}(x) > 0.45$], a straight line is realized. The extrapolated value of δ_{FeSb} is 0.78 mm/sec, which is larger than the predicted value of 0.66 mm/sec. In the range of $C_{Fe}(x) < 0.45$, however, the isomer shifts depart completely from the predicted straight line.

TABLE I. Work function $\phi(V)$, electron density on the Wigner-Seitz cell, n, molar volume V, and bulk modulus K of Fe and Sb.

	$\phi(V)$	n	V (cm^3)	K (10^{11} N/m^2)
Fe	4.93	5.55	7.1	1.683
Sb	4.40	2.00	18.2	0.383

Miedema and van der Woude have introduced a volume-mismatch term having the following form for alloys with *strained structures*,[8,11]

$$\delta_{vol} = \frac{0.615K_A}{0.615K_A + K_{Fe}} \frac{V_A - V_{Fe}}{V_{Fe}} \frac{\partial(\delta)}{\partial(\ln V)} \ , \quad (4)$$

where K is the bulk modulus, V is the molar volume, and $[\partial(\delta)/\partial(\ln V)]$ is the volume dependence of the isomer shift obtained from high-pressure measurements. All the reported values of $[\partial(\delta)/\partial(\ln V)]$ are close to 1 mm/sec, and the most frequently quoted value is 1.33 mm/sec.[12] It should be noted that the sign of δ_{vol} is determined by $(V_A - V_{Fe})$ alone.

It is instructive to mention vapor-quenched amorphous Fe_xB_{100-x} ($0 < x \leq 90$) alloys, whose isomer shifts have a qualitatively similar dependence on composition as amorphous Fe-Sb; in particular, there is also a clear departure on the B-rich side ($x < 50$) from the prediction of the Miedema—van der Woude model. Hoving *et al.*[11] indicated that with the inclusion of a volume-mismatch term (4) (which is negative because B has a smaller molar volume) on the B-rich side, the value of $\delta_{FeB} + \delta_{vol}$ is reasonably close to the experimental results. They con-

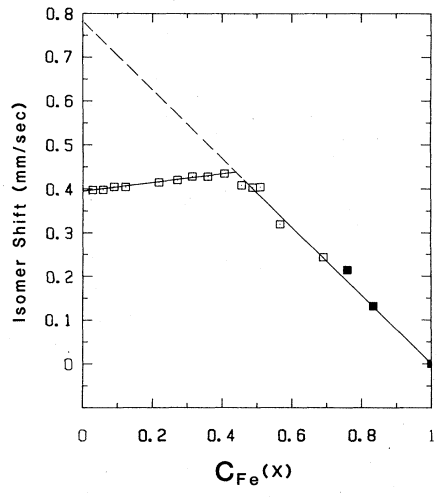

FIG. 4. Isomer shift of amorphous Fe-Sb alloys as a function of Fe surface-area concentration C_{Fe} defined in the text.

cluded therefore that in Fe-B metallic glass, the B-rich side has a strained structure, whereas the Fe-rich side is densely packed but strain free.

However, the volume-mismatch term cannot account for the data of amorphous Fe-Sb on the Sb-rich side. This is because the molar volume is larger in Sb and a positive value of $\delta_{\rm vol} \simeq 0.26$ mm/sec is obtained for the Fe-Sb alloy, but the term needed to explain the departure from the model should be negative. It is further noted that the composition dependence of the isomer shift of all the amorphous Fe—*sp*-element (B, Si, Ge, and Sn) (Refs. 11 and 13—15) systems is qualitatively similar to that of Fe-Sb. Questions arise as to whether the volume-mismatch term is even applicable in Fe-B, despite its apparent agreement with the data. It has been reported that in many Fe—transition-metal amorphous alloys, Eq. (2) alone can reasonably account for the isomer shift over the entire composition range[9,10,16] due, presumably, to the metallic nature of the materials. For the Fe—*sp*-element amorphous systems, it seems reasonable to expect this is so at the Fe-rich side. An additional term, however, other than the volume-mismatch term, would be needed for the data in the Fe-poor region. Since the data, as shown in Fig. 4, are close to being linear in both regions, one can easily deduce this extra term. For the Fe-Sb alloys, the following relations are applicable,

$$\delta(x)=\begin{cases}\delta_{FeSb}[1-C_{Fe}(x)]+[-0.39+0.87C_{Fe}(x)], & 0<C_{Fe}\leq 0.45\\ \delta_{FeSb}[1-C_{Fe}(x)], & 0.45<C_{Fe}\leq 1\end{cases} \tag{5}$$

where $\delta_{FeSb}=0.78$ mm/sec. The fact that a new term is necessary in the amorphous Fe—*sp*-element alloys suggests that the mechanism should be related to the *sp* electrons in these elements. One of the possible contributions to this term is the hybridization of the $3d$ band of Fe with the valence band of the *sp* elements. The hybridization effect obviously becomes less and less important as the content of the *sp* element is reduced. This explains why the new term decreases with decreasing *sp*-element concentration. In its crystalline form, Sb is a semimetal with a small band overlap of about 0.025 eV, while amorphous Sb was found to be a semiconductor[17,18] and its pseudogap is as large as that of amorphous Ge. Electron-spin-resonance[19] and x-ray photoemission spectroscopy[20] studies have indicated that the *d* levels of transition-metal impurities are strongly hybridized with the *sp*-band states of a semiconductor matrix.

B. Electric quadrupole interaction

Mössbauer spectra of the samples which remain paramagnetic at 300 K, as well as their quadrupole-splitting distribution, are shown in Fig. 1. The fitting of the experimental data, based on Window's method, provides the quadrupole splitting (QS) and its distribution. The spectra of Fe_xSb_{100-x} $(5\leq x\leq 63)$ show a gradual change of spectrum asymmetry (different intensities of the two absorption peaks) which can be accounted for by a correlation between the isomer shift δ and QS. In our fitting procedure, a linear correlation is used, i.e.,

$$\delta=\delta_0+\beta(\Delta_{QS}-\Delta_{QS_0})\ . \tag{6}$$

The value of β obtained is positive at low Fe concentration and changes into negative values starting from 45 at.% of Fe. This correlation is commonly observed in amorphous alloys.

The composition dependence of the mean QS at 4.2 and 300 K is shown in Fig. 5 as open circles and squares, respectively. Both curves show a shallow minimum at about $x=30$. The values at 4.2 K are higher than those at 300 K. The fact that the two curves are parallel indicates that for all compositions the temperature dependence of the effective field gradients are nearly the same. The features of the mean QS are similar to that in Fe-Si (Refs. 13 and 21) and Fe-Ge (Ref. 14) amorphous alloys. One observes from Figs. 1 and 5 that the QS distribution and the mean QS do not vary much over the range of $5\leq x\leq 50$. This is an indication that the atomic packing scheme in this range remains the same. However, as the Fe concentration increases beyond $x=50$, a shoulder is gradually developed at the high-QS side of the distribution, implying that some of the Fe atoms start to take positions with more asymmetric local environments. Anoth-

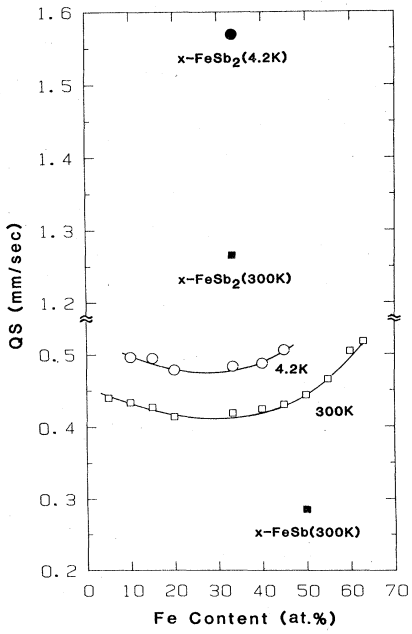

FIG. 5. Mean quadrupole splitting of amorphous Fe-Sb alloys as a function of Fe concentration at 4.2 and 300 K. Open squares and circles are data of amorphous samples and solid squares and circles are data of crystalline samples.

er point of interest is that the full width of the QS distribution is as large as, or even larger than, the mean QS itself. The ratio

$$\frac{(\langle V_{zz}^2\rangle-\langle\,|V_{zz}|\,\rangle^2)^{1/2}}{\langle\,|V_{zz}|\,\rangle}$$

is about 0.45—0.55. This means that structural fluctuations or the degree of disorder is rather large in Fe-Sb, while for Fe-Si amorphous alloys this width is much smaller than the mean QS in the range of $x<50$.[13] Overall, our results of $P(\mathrm{QS})$ are quite similar to the distribution expected from a model of random atomic packing.[22–24]

A particularly striking feature of Fe-Sb comes from the discovery that the QS value of crystalline x-$FeSb_2$ is larger than that of its amorphous counterpart, a-$FeSb_2$, at both 4.2 and 300 K, by a factor of 3, as shown in Figs. 5 and 6. To the best of our knowledge, this is the largest difference in QS ever found in Fe—*sp*-element and Fe—transition-element amorphous alloys. Steger *et al.*[25] have investigated the Mössbauer effect of crystalline x-$FeSb_2$ over the temperature range of 6.4—560 K with the motivation of explaining the significant change in QS with temperature. It has been found that the temperature dependence of x-$FeSb_2$ can be described as a sum of valence contributions and lattice contributions,

$$\Delta_{\mathrm{QS}}(T)=\Delta_{\mathrm{QS}}^{\mathrm{val}}(T)+\Delta_{\mathrm{QS}}^{\mathrm{lat}}(T) \tag{7}$$

and with the explicit temperature dependence of

$$\Delta_{\mathrm{QS}}^{\mathrm{val}}(T)=\Delta_{\mathrm{QS}}^{\mathrm{val}}(0)\tanh[E/2k_BT]\,, \tag{8}$$

$$\Delta_{\mathrm{QS}}^{\mathrm{lat}}(T)=\Delta_{\mathrm{QS}}^{\mathrm{lat}}(0)+T\frac{d}{dT}[\Delta_{\mathrm{QS}}^{\mathrm{lat}}(T)]\,, \tag{9}$$

where $\Delta_{\mathrm{QS}}^{\mathrm{val}}(0)=0.716$ mm/sec, $\Delta_{\mathrm{QS}}^{\mathrm{lat}}(0)=0.864$ mm/sec, $E=0.033$ eV, and $d[\Delta_{\mathrm{QS}}^{\mathrm{lat}}(T)]/dT=-0.472\times10^{-4}$ mm/sec K. In the temperature range of 4.2—300 K, the temperature dependence of the lattice contribution is negligible.

Our data for x-$FeSb_2$ and a-$FeSb_2$ and values from relations (8) and (9) for x-$FeSb_2$ are summarized in Table II.

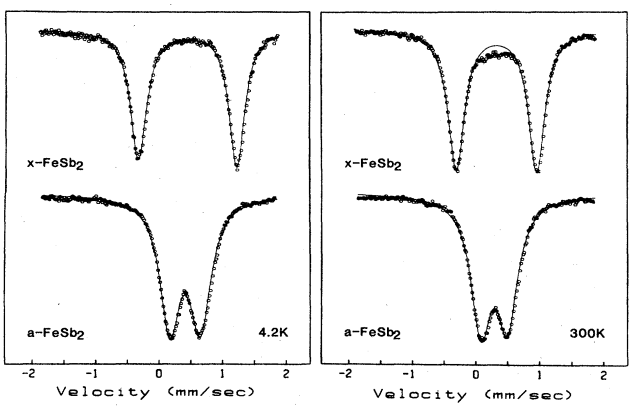

FIG. 6. Mössbauer spectra of amorphous $FeSb_2$ and crystalline $FeSb_2$ at 4.2 and 300 K.

TABLE II. Electric quadrupole splitting Δ_{QS}, quadrupole splitting due to valence contribution $\Delta_{\mathrm{QS}}^{\mathrm{val}}$, and quadrupole splitting due to lattice contribution $\Delta_{\mathrm{QS}}^{\mathrm{lat}}$ of x-$FeSb_2$ and a-$FeSb_2$ at 4.2 and 300 K.

	T (K)	$\Delta_{\mathrm{QS}}(T)$ (mm/sec)	$\Delta_{\mathrm{QS}}^{\mathrm{val}}(T)$ (mm/sec)	$\Delta_{\mathrm{QS}}^{\mathrm{lat}}(T)$ (mm/sec)
x-$FeSb_2$	4.2	1.568	0.716	0.864
	300	1.265	0.404	0.850
a-$FeSb_2$	4.2	0.484		
	300	0.419		

The value of $\Delta_{\mathrm{QS}}=0.484$ mm/sec observed in a-$FeSb_2$ is much smaller than $\Delta_{\mathrm{QS}}^{\mathrm{val}}$, $\Delta_{\mathrm{QS}}^{\mathrm{lat}}$, and Δ_{QS} of x-$FeSb_2$. Hence the local environment of a-$FeSb_2$ is entirely different from that of x-$FeSb_2$. The structure of x-$FeSb_2$ is of orthorhombic marcasite type (e.g., FeS_2), a structure far from being closely packed, each Fe atom being octahedrally coordinated by six Sb atoms. It is likely that the structure of a-$FeSb_2$ can be described by the dense-random-packing model. The high coordination number around Fe significantly reduces the mean QS. According to Steger *et al.*, the unusually strong temperature dependence of QS in x-$FeSb_2$ comes primarily from the valence-electron contribution, as a result of the thermally activated electrons crossing an energy gap of about 0.033 eV. In amorphous a-$FeSb_2$, the much weaker temperature dependence of QS reflects a much different valence-electronic structure from that in x-$FeSb_2$.

In contrast to the case of $FeSb_2$, the mean QS of x-FeSb is much smaller than that of a-FeSb (Fig. 5). The structure of x-FeSb is of NiAs type, in which each Fe has eight neighbors, six Fe and two Sb. Judging from the mean QS, this arrangement is clearly not realized in a-FeSb. Thus, we see no correlation in local structure between amorphous $FeSb_2$, FeSb, and their crystalline counterparts. The results argue strongly against the conjecture that the amorphous structure may retain a considerable degree of the local order found in crystalline counterparts as suggested by some models, at least for the Fe-Sb system.

C. Magnetic properties and magnetic hyperfine interaction

The magnetic ordering temperatures of the samples, including both the ferromagnetic ordering temperatures of the Fe-rich samples and the spin-glass freezing temperatures of the samples with $x<60$, are shown in Fig. 7. Like other Fe—*sp*-element amorphous alloys (e.g., Fe-B,[26] Fe-Si, etc.), the values of T_c are a few hundred degrees Kelvin higher than those of the Fe—early-transition-element alloys (e.g., Fe-Ti,[27] Fe-Zr,[16] Fe-Hf,[28] etc.) with the same Fe concentration. The values of T_c of the samples with $x\geq65$ were determined from the onset of the magnetic hyperfine interaction by using the zero-velocity thermal-scan method, while those of others were obtained from magnetization measurements.

Magnetization measurements at 5 K as a function of

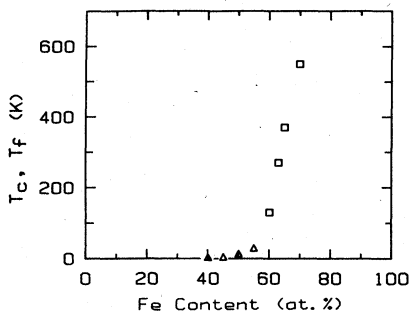

FIG. 7. The ferromagnetic ordering temperatures (T_c), denoted as squares, and spin-freezing temperatures (T_f), denoted as triangles, of amorphous Fe-Sb.

external fields indicates that the Fe-rich samples ($x > 60$) are mainly ferromagnetic, whereas the samples with $x < 55$ are not. It is also found that the T_c of samples near $x = 60$ are not as well defined as those in the higher-Fe-concentration region. We believe that this is caused by large magnetic inhomogeneities as evidenced in the unusually broad magnetic hyperfine field distribution in $Fe_{60}Sb_{40}$ as shown in Fig. 2. It has been shown[29] that the fluctuation in the magnetic exchange interaction (J) introduced by the structural disorder induces a local fluctuation in the magnetic ordering, thereby broadening or even smearing out the phase transition. Another possible effect of structural disorder is the introduction of antiferromagnetic exchange interaction. The competing ferromagnetic and anitferromagnetic exchange interactions may result in spin-glass behavior, which has been observed in samples with $x < 60$. Shown in Fig. 8 are the magnetization-versus-temperature curves of $Fe_{45}Sb_{55}$ and $Fe_{50}Sb_{50}$ under an external field of 30 Oe for increasing and decreasing temperatures. During the measurements, the samples were first cooled to about 1.6 K under zero field and then the magnetic field was applied. A peak, observed at T_f, as well as the irreversible behavior between the zero-field-cooled temperature-increasing curve and the field-cooled temperature-decreasing curve, are characteristics of a spin glass.

The Mössbauer spectra and the deduced magnetic hyperfine field distributions of some magnetic samples at 4.2 K are shown in Fig. 2. Samples with iron concentration above 50 at.% show magnetic hyperfine splitting at 4.2 K, while those with iron concentrations below 45 at.% exhibit broad doublets.

As can be seen from the spectra, the intensities of the second and fifth line are suppressed, indicating that the spin orientations tend to be out of the sample plane. This perpendicular anisotropy is most likely caused by stresses from the substrate through magnetostriction.[30] As a comparison, we include the Mössbauer spectrum of a bcc crystalline $Fe_{85}Sb_{15}$ sample (Fig. 9), where similar spin anisotropy also exists. Under an external field of about 1 kOe applied in the $Fe_{70}Sb_{30}$ sample plane, the magnetic moments orient substantially in the sample plane (Fig. 10). This is an indication that the sample is ferromagnetic and soft.

The Mössbauer spectra shown in Fig. 2 exhibit an

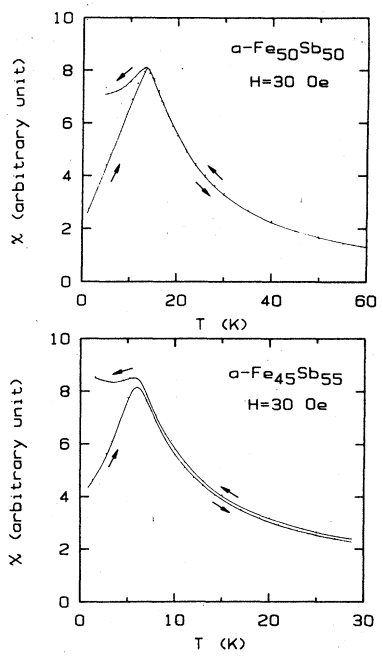

FIG. 8. Magnetic-susceptibility—versus—temperature curves with external field $H = 30$ Oe for $Fe_{45}Sb_{55}$ and $Fe_{50}Sb_{50}$. Arrows represent increasing and decreasing temperature measurement.

asymmetry of line intensities with respect to the isomer shift. This is caused by a correlation between the isomer shift and the hyperfine field. A linear correlation is assumed in fitting the spectra and deducing the hyperfine field distribution $P(H)$, i.e., $\delta = \delta_0 + bH$, where b is found to be negative in all cases, for $Fe_{80}Sb_{20}$, b is about -0.0016 mm/kOe.

The effective magnetic hyperfine field versus Fe concentration at 4.2 K is shown in Fig. 11. H_{eff}, and hence the effective magnetic moment, rises sharply with increasing Fe concentration at about $x_c = 47$. From the magnetization data which will be discussed in a future paper, we find spin-glass-like behavior from $x = 40$ to 60 and no ap-

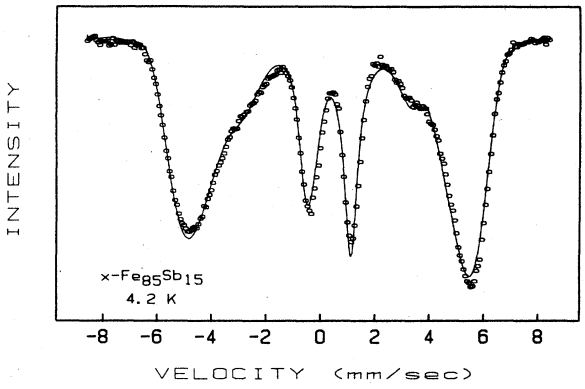

FIG. 9. Mössbauer spectrum of crystalline bcc $Fe_{85}Sb_{15}$ at 4.2 K.

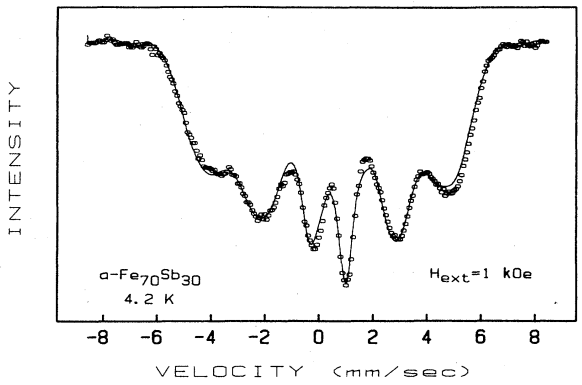

FIG. 10. Mössbauer spectrum of amorphous $Fe_{70}Sb_{30}$ at 4.2 K with an external magnetic field of about 1 kOe applied in the sample plane.

preciable magnetic ordering for $x < 40$ down to 4.2 K, but paramagnetic characteristics exist in some samples with $x < 40$.

There is much debate concerning the appearance and evolution of magnetic moment in amorphous alloys from the standpoint of localized moment and itinerant models. Work has been done on amorphous alloys such as Fe-Si, Fe-Ge, and Fe-Sn (Refs. 21 and 31—35) to elucidate the magnetic behavior of these Fe—*sp*-element amorphous alloys (Si, Ge, and Sn are all group-IV*B* elements in the Periodic Table). Critical concentrations x_c, where an effective magnetic moment appears, are about the same for Fe-Si and Fe-Ge, namely $x_c = 40$, and for Fe-Sn, about 30. These values are lower than $x_c = 47$ for Fe-Sb in which Sb is a group-V*B* *sp* element, having one more *p* valence electron than Si, Ge, and Sn.

In the rigid-band model, the disappearance of the Fe magnetic moment is a consequence of the filling of the 3*d* band of Fe by valence electrons of the *sp* element. The magnetic moment of pure bcc Fe (2.2 Bohr magnetons) and number of holes (2.6 holes) in the *d* band will be reduced by gradually adding an *sp* element. A simple calculation gives the critical concentration $x_c = 43$ for Fe-Si, Fe-Ge, and Fe-Sn systems and $x_c = 53$ for Fe-Sb systems.

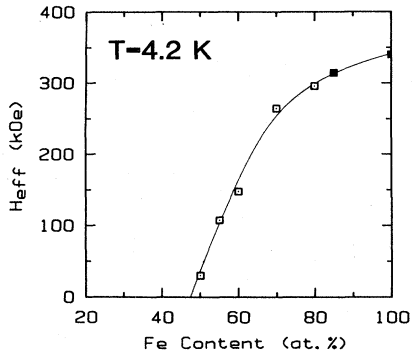

FIG. 11. Effective magnetic hyperfine fields of amorphous Fe-Sb and crystalline Fe-Sb alloys as a function of Fe concentration at 4.2 K.

Hence, the model does give a higher critical concentration for the Fe-Sb system. The actual experimental values are all less than the predicted ones. Since this model is a homogeneous magnetism model, we cannot expect it to account for the magnetic inhomogeneity occurring in Fe-Sb and other amorphous alloys. Here the magnetic inhomogeneity is manifested by the coexistence of magnetic and nonmagnetic atoms in some samples close to the critical concentration such as $Fe_{50}Sb_{50}$ and the very broad magnetic hyperfine field distribution occurring in $Fe_{60}Sb_{40}$.

The model which has been widely favored and we feel more appropriate for Fe-Sb amorphous system is the nearest-neighbor (NN) coordination model (a localized-moment model).[21] Effective Fe magnetic moments and hyperfine fields are determined by the number of Fe atoms in the first-nearest-neighbor shell around a central Fe atom. It has been suggested in Fe-Si amorphous system[21] that, in order for the Fe moment to appear, n has to be larger than six for high Fe concentration and about seven for Fe-poor samples. Similarly, in Fe-Y amorphous alloys,[31] the Fe moment would increase with Fe neighbors from a few tenths of a Bohr magneton with $n = 6$ up to 2 Bohr magnetons with $n > 10$. This model naturally explains the magnetic inhomogeneity and appearance of paramagnetic moments below the critical concentration in Fe-Sb by attributing them to structural fluctuations, i.e., fluctuation of the number of Fe atoms and the distance of the NN shell around a central Fe atom. The monotonic increase of H_{eff} with Fe concentration is also compatible with this model.

Although the NN coordination model offers consistent explanations for various amorphous systems, some features of itinerant models need to be taken into account also. The hybridization between the 3*d* band of Fe and *sp* conduction band of the *sp*-element can hardly be ruled out in Fe—*sp*-element alloys and should influence the behavior of the Fe magnetic moments. Generally, the hybridization effect will make the *d* band wider and, therefore, reduce the magnetic moment of Fe.

An interesting feature of Fe-Sb alloys is that H_{eff} changes smoothly as Fe-Sb changes from an amorphous to a crystalline phase, suggesting that the hyperfine field is not sensitive to the structural disorder in the range of $80 \leq x \leq 85$. It is apparent from the width of the hyperfine field distribution (see discussion below) that $Fe_{80}Sb_{20}$ is more magnetically homogeneous than other samples. The effect of structural disorder on the magnetic behavior in $Fe_{80}Sb_{20}$ is evidently comparable to the effect of chemical disorder introduced by random substitution of Sb into Fe sites in the bcc Fe matrix. In other Fe—*sp*-element amorphous alloys such as Fe-B (Ref. 26) and Fe-Si (Ref. 37), a continuous curve of H_{eff} connecting Fe-rich amorphous alloys and pure α-Fe is also observed. On the contrary, an abrupt increase in H_{eff} normally occurs in Fe—early-transition-element amorphous alloys, namely Fe-Ti,[27] Fe-Hf,[28] Fe-Mo,[38] etc.

Using Fourier-series methods, the hyperfine field distribution of various spectra at 4.2 K have been analyzed. The quadrupole interaction is neglected, although poorly justified in the case of $Fe_{50}Sb_{50}$, as can be seen from the

spectrum. Care should be taken in evaluating and analyzing these very wide $P(H)$. It would be hazardous to overemphasize the detailed structure of $P(H)$ due to a variety of distortions, only the general shape of the $P(H)$ can provide useful information. Except in the case of $Fe_{50}Sb_{50}$, the amplitude vanishes at about 380 kOe, corresponding to the highest magnetic moment in these samples. Reducing the Fe concentration not only moves the peak of $P(H)$ to the low-field side, but also increases the width of $P(H)$ substantially. For example, the width of $P(H)$ of $Fe_{80}Sb_{20}$ is only about 120 kOe, while the $P(H)$ of $Fe_{60}Sb_{40}$ shows appreciable amplitude over a large range of $0 < H < 300$ kOe. Based on the assumption that the hyperfine field distribution in substitutional alloys such as Fe-Sb, Fe-Si, Fe-Ge, and Fe-Sn is correlated to the distribution of coordination number of Fe around the Fe atom, it can be concluded that by reducing the Fe concentration the variation in the number of Fe atoms in the NN shell around a given Fe atom increases, and the system becomes more and more magnetically inhomogeneous. The $P(H)$ of $Fe_{50}Sb_{50}$ is similar to that of $Fe_{50}Si_{50}$ and $Fe_{45}Ge_{55}$. The large peak between $0 < H < 50$ kOe is a consequence of the electric quadrupole interaction. The coexistence of magnetic and nonmagnetic Fe atoms in the alloy make the $P(H)$ analysis unreliable. We estimate, however, that the fraction of nonmagnetic Fe atoms is about 40%.

IV. SUMMARY AND CONCLUSION

By using a vapor-quench method, we have successfully fabricated amorphous Fe_xSb_{100-x} alloys with a wide composition range ($3 \leq x \leq 80$). The hyperfine interactions as well as magnetic properties in this system have been studied systematically using Mössbauer spectrometry and magnetization measurements.

The isomer shifts as a function of concentration show two distinct regions separating the Fe-rich and Sb-rich sides. The Miedema—van der Woude model works well at the Fe-rich side, but a large discrepancy in the Sb-rich side suggests a new term characteristic of *sp* elements such as Sb is necessary in that model. It is expected that the inclusion of that term can explain the similar isomer shift behavior in other Fe—*sp*-element amorphous systems.

The concentration dependence of quadrupole splitting and its distribution reveals a similar atomic packing scheme from the Sb-rich side to $x = 55$, but the local structure of amorphous a-$FeSb_2$ is entirely different from that of crystalline x-$FeSb_2$, as indicated in the extremely large difference in quadrupole splitting (a factor of 3).

At $x > 65$, samples exhibit mainly ferromagnetic ordering at low temperatures, while below $x = 60$, spin-glass behavior was observed. Magnetic hyperfine fields, and hence effective magnetic moments, increase monotonically with Fe concentration at about $x = 47$. A very broad magnetic hyperfine field distribution around $x = 60$ indicates a large magnetic inhomogeneity in that region that is responsible for the magnetic fluctuation.

ACKNOWLEDGMENT

This work was supported by the National Science Foundation under Grant No. DMR-82-05135.

*Present address: W. M. Keck Laboratory of Engineering Materials, California Institute of Technology, Pasadena, CA 91125.

[1]See, for example, H. H. Lieberman, in *Amorphous Metallic Alloys,* edited by F. E. Luborsky (Butterworths, London, 1983), pp. 26—41.

[2]See, for example, *Handbook of Thin Film Technology,* edited by L. I. Maissel and R. Glang (McGraw-Hill, New York, 1970).

[3]C. L. Chien, in *Nuclear and Electron Resonance Spectroscopies Applied to Materials Science,* edited by E. N. Kaufmann and G. K. Shenoy (North-Holland, New York, 1981), p. 157.

[4]P. Panissod, J. Durand, and J. I. Budnick, Nucl. Instrum. Methods **199**, 99 (1982).

[5]U. Gonser and R. Preston, in *Glassy Metals II,* edited by H. Beck and H.-J. Güntherodt, Springer Series in Topics in Applied Physics (Springer, Berlin, 1983), Vol. 53, p. 93.

[6]T. Shigematsu, T. Shinjo, Y. Bando, and T. Takada, J. Magn. Magn. Mater. **15-18**, 1367 (1980).

[7]M. Hashimoto, H. Sugibuchi, and K. Kambe, Thin Solid Films, **98**, 197 (1982).

[8]A. R. Miedema and F. van der Woude, Physica B&C **100**, 145 (1980).

[9]A. M. van der Kraan and K. H. J. Buschow, Phys. Rev. B **25**, 3311 (1982).

[10]A. M. van der Kraan and K. H. J. Buschow, Phys. Rev. B **27**, 2693 (1983).

[11]W. Hoving, F. van der Woude, K. H. J. Buschow, and I. Vincze, in *Liquid and Amorphous Metals V. Proceedings of the Fifth International Conference on Liquid and Amorphous Metal,* edited by C. N. J. Wagner and W. L. Johnson (North-Holland, Amsterdam, 1984), p. 421.

[12]R. Ingalls, F. van der Woude, and G. A. Sawatzky, in *Mössbauer Isomer Shift,* edited by G. K. Shenoy and F. E. Wagner (North-Holland, Amsterdam, 1978), p. 405.

[13]C. Bansal, S. J. Campbell, and A. M. Stewart, J. Magn. Magn. Mater. **27**, 195 (1982).

[14]O. Massenet and H. Daver, Solid State Commun. **21**, 37 (1977).

[15]M. Piecuch, Chr. Janot, and G. Marchal, J. Phys. (Paris) Colloq. **41**, C1-251 (1980).

[16]K. M. Unruh and C. L. Chien, Phys. Rev. B **30**, 4968 (1984).

[17]J. J. Hauser, Phys. Rev. B **9**, 2623 (1974).

[18]J. J. Hauser, Phys. Rev. B **11**, 738 (1975), and references therein.

[19]G. W. Ludwig and H. H. Woodbury, in *Electron Spin Resonance in Semiconductors,* Vol. 13 of *Solid State Physics,* edited by F. Seitz and D. Turnbull (Academic, New York, 1962), p. 223.

[20]J. Fukushima, K. Tamura, H. Endo, K. Kishi, S. Ikeda, and

S. Minomura, in *Tetrahedrally Bonded Amorphous Semiconductors (Yorktown Heights)*, Proceedings of the International Conference, edited by M. H. Brodsky, S. Kirkpatrick, and D. Wearie (AIP, New York, 1974), p. 108.
[21]G. Marchal, Ph. Mangin, M. Piecuch, and Chr. Janot, J. Phys. (Paris) Colloq. **37**, C6-763 (1976).
[22]G. Czjzek, J. Fink, F. Götz, H. Schmidt, J. M. D. Coey, J.-P. Rebouillat, and A. Liénard, Phys. Rev. B **23**, 2513 (1981).
[23]M. E. Lines, Phys. Rev. B **20**, 3729 (1979).
[24]P. Heubes, D. Korn, G. Schatz, and G. Zibold, Phys. Lett. **74A**, 267 (1979).
[25]J. Steger and E. Kostiner, J. Solid State Chem. **5**, 131 (1972).
[26]C. L. Chien and K. M. Unruh, Phys. Rev. B **25**, 5790 (1982).
[27]S. H. Liou and C. L. Chien, J. Appl. Phys. **55**, 1820 (1984).
[28]S. H. Liou, G. Xiao, J. N. Taylor, and C. L. Chien, J. Appl. Phys. **57**, 3536 (1985).
[29]A. B. Harris, J. Phys. C **7**, 1671 (1974).
[30]Hang Nam Ok and A. H. Morrish, Phys. Rev. B **22**, 4215 (1980).
[31]Ph. Margin, M. Piecuch, G. Marchal, and Chr. Janot, J. Phys. F **8**, 2085 (1978).
[32]D. Bloch, Ph. Mangin, G. Marchal, and Chr. Janot, Solid State Commun. **25**, 555 (1978).
[33]P. Terzieff, K. Lee, and N. Heiman, J. Appl. Phys. **50**, 1031 (1979).
[34]B. Rodmacq, M. Piecuch, Chr. Janot, G. Marchal, and Ph. Mangin, Phys. Rev. B **21**, 1911 (1980).
[35]D. Tierlinck, M. Piecuch, J. F. Geng, G. Marchal, Ph. Mangin, and Chr. Janot, IEEE Trans. Magn. **MAG-17**, 3079 (1981).
[36]J. Chappert, J. M. D. Coey, A. Lienard, and J. P. Rebouillat, J. Phys. F **11**, 2727 (1981).
[37]G. Marchal, Ph. Mangin, M. Piecuch, Chr. Janot, and J. Hubsch, J. Phys. F **7**, L165 (1977).
[38]C. L. Chien, S. H. Ge, S. H. Liou, and G. Xiao, J. Magn. Magn. Mater. (to be published).